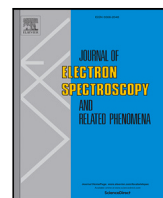




Contents lists available at ScienceDirect

Journal of Electron Spectroscopy and Related Phenomena

journal homepage: www.elsevier.com/locate/elspec

Observation and theory of strong circular dichroism in angle-revolved photoemission from graphite

Peter Krüger^{a,*}, Fumihiko Matsui^b

^a Graduate School of Engineering and Molecular Chirality Research Center, Chiba University, Chiba 263-8522, Japan

^b UVSOR Synchrotron Facility, Institute for Molecular Science, Okazaki, 444-8585, Japan

ARTICLE INFO

Keywords:

Graphene
Band structure
Photoemission
Circular dichroism
Multiple scattering

ABSTRACT

Experimental angle-resolved photoemission spectra (ARPES) and its circular dichroism (CD) from a graphite surface are reported together with calculations in the one-step model of photoemission. For photoelectrons emitted with surface parallel momentum k_{\parallel} perpendicular to the incoming light, a strong and complex CD signal is observed and analyzed along the Γ -K and Γ -M lines of the Brillouin zone. Calculations using real-space multiple scattering theory agree well with the data both for the total ARPES and the CD intensity maps. In the independent atomic approximation, i.e. when photoelectron scattering is neglected, the total ARPES intensity map is still well described, but not the CD. We find that photoelectron scattering makes a large contribution to the CD signal and may change its sign. Moreover, the CD of the bands depends strongly on photon energy, while this is much less the case for the total ARPES intensity. The present findings show that an accurate description of the photoemission final state, including photoelectron scattering effects, is crucial for understanding the CD in ARPES from surfaces and two-dimensional materials.

1. Introduction

Low-dimensional materials and surfaces feature novel quantum phenomena such as the Rashba effect and Dirac cones, which are promising for future electronic devices. Angle Resolved Photo-Emission Spectroscopy (ARPES) gives direct access to the 2D band structure of these materials [1,2]. In combination with spin-resolution and/or circular polarized light, the spin-polarization and spin-orbit coupling (SOC) of the bands can be probed [3]. Recent instrumental advances such as photoelectron momentum microscope [4,5] and novel theoretical concepts including orbital tomography [6], have made ARPES more powerful and versatile for probing the valence electronic structure of surfaces, 2D-materials and molecular films [7–9]. ARPES involves the excitation of an electron from an initial valence state to a final continuum state and the ARPES intensity is given by the square of the optical transition matrix element between initial and final state. Most ARPES users are only interested in initial state properties, e.g. the band dispersion and/or orbital character of the valence states. The fact that the ARPES intensity also depends on the final state wave function, might then be considered a nuisance rather than a source of information. When ARPES is used for band mapping, the dependence on the final state wave can be disregarded, because the peak positions alone determine the band dispersion $E(\mathbf{k})$ and the ARPES intensities need not be analyzed. However, the ARPES intensities contain rich

information about the valence electron wave functions. If the ARPES intensities are to be analyzed, the optical transition matrix elements need to be calculated, and a model for the final state wave is required. The most simple model is the plane wave approximation (PWA), where the photoemission final state is taken as a single plane wave, i.e. a free electron eigenstate [10]. The PWA completely neglects the crystal potential in the final state calculation. Nonetheless, the PWA can be surprisingly good. For example, it is used in the orbital tomography method [6], which has been very successful for explaining ARPES intensity patterns of π -type molecular orbitals of organic molecules [9]. In the PWA, distorted wave effects and photoelectron scattering are neglected. The former effect can be dealt with the independent atomic center approximation [11,12], and the latter with multiple scattering theory (MST) [13]. These methods build up the final state wave from interfering atom-centered waves. This requires space partitioning into atomic cells which is difficult without making strong approximation on the potential shape. Indeed, multiple scattering calculations are commonly carried out together with the muffin-tin approximation, which is good for close-packed bulk crystals, but of limited accuracy for most other materials [14]. Full potential versions of MST have been developed by various authors [15–17], but their performance for ARPES of molecules and low-dimensional systems remains to be shown.

* Corresponding author.

E-mail address: pkruiger@chiba-u.jp (P. Krüger).

<https://doi.org/10.1016/j.elspec.2022.147219>

Received 13 March 2022; Accepted 12 June 2022

Available online 5 July 2022

0368-2048/© 2022 Elsevier B.V. All rights reserved.

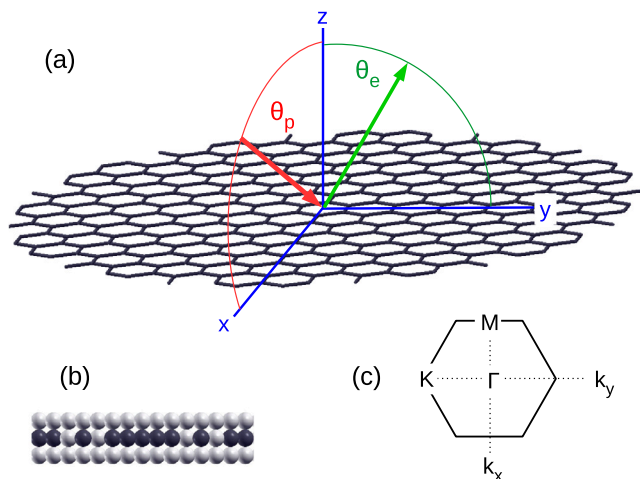


Fig. 1. (a) Experimental geometry for $\mathbf{k}_{\parallel} = (0, k_y)$ ARPES scans. (For $(k_x, 0)$ scans, the sample is rotated by 90° about the surface normal.) The incoming light and the photoemission direction are indicated by red and green arrows and their polar angles w.r.t. the surface normal are $\theta_p = 60^\circ$ and θ_e , respectively. A stick-model of the graphene cluster used in the calculation is also shown. (b) Side view of the calculation cluster with carbon atoms (black balls) and empty spheres (white balls). (c) Brillouin zone of graphene.

ARPES from graphite has been studied for long [18] but some effects, e.g. the 4π -periodicity along k_z , were explained only recently [19]. Here we report the observation and theoretical modeling of a strong and complex circular dichroism (CD) signal in the ARPES of graphite. In absorption spectroscopy, CD is routinely measured and well understood. A non-zero CD signal is a direct sign that the system lacks either space- or time-inversion symmetry, i.e. that it is chiral or magnetic. In ARPES, however, the situation is much complicated by the fact that the electron emission direction adds another axis to the problem apart from the symmetry axes of the system and the helicity vector of the light. If the experimental system, composed of sample, incident beam and photoelectron emission vector, lacks mirror symmetry, then left and right helicity are not longer symmetry equivalent, and circular dichroism in angular distribution may occur [20]. Since the CD in ARPES is a powerful probe for chiral and topological electronic states [3], it is important to understand its origin and to distinguish CD due to the symmetry of the initial state wave function, and CD that is induced by the experimental geometry.

In this paper, we report the observation of strong CD in ARPES from a graphite surface. The data is compared with calculations based on the one-step model of photoemission with both initial and final states computed with MST. We obtain very good agreement with the data for the ARPES intensity map. Importantly, the strongly band- and k -dependent CD pattern is well reproduced. In order to assess the origin of the CD, we also perform calculations in the independent atomic center approximation (IACA), i.e. by neglecting the scattering of the outgoing photoelectron. The differences between MST and IACA are small for the ARPES map, but very large for the CD, where the IACA fails to reproduce the data. This shows that photoelectron scattering effects make a large contribution to CD in ARPES and that an accurate description of the final state wave function is indispensable.

2. Experimental and theoretical details

A graphite single crystal of 1-mm diameter was mounted on a sample holder and cleaved just before introducing it into ultrahigh vacuum for measurements [19]. The surface quality was checked by LEED, AES, and XPS measurements and no contamination was detected. The valence band dispersion as a function of photon energy was measured by a concentric hemispherical analyzer at the polarization variable soft

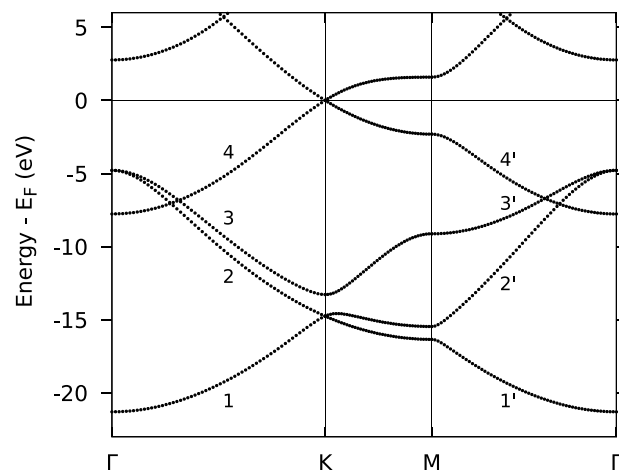


Fig. 2. Band structure of graphene obtained with the LMTO code in the local density approximation. The occupied bands are numbered for easy reference.

X-ray beamline XA03DA of Swiss Light Source, Switzerland [21]. Ellipsoidal polarized light with a polarization up to 70% was available [19]. The analyzer was centered at 60° from incident light. The acceptance angle mode of the analyzer was $\pm 30^\circ$ vertical to the plane including the incident light, its electric vector, and the direction to the center of the analyzer entrance slit.

The experimental geometry is sketched in Fig. 1a. Circularly polarized light of energy $h\nu = 80$ eV is impinging on C(0001) at $\theta_p = 60^\circ$ from the surface normal. The photoelectrons are collected perpendicular to the scattering plane. First, the incident light beam is in the xz -plane (with $x > 0$) and the photoelectrons are emitted in the yz -plane, as shown in Fig. 1a. In this case, the 2D momentum of the electrons is $\mathbf{k}_{\parallel} = (0, k_y)$, along the Γ -K line. Second, the sample is rotated by 90° around the surface normal. Now the light is incident in the yz -plane (with $y < 0$) and the momenta $\mathbf{k}_{\parallel} = (k_x, 0)$ along the Γ -M line are probed.

The calculations are carried out using the real-space multiple scattering method developed by Krüger et al. [22]. The graphite surface is modeled with a cluster of 336 C atoms in one graphene layer, as shown in Fig. 1a. Because of the weak van der Waals coupling between the graphene sheets, and because we focus on the \mathbf{k}_{\parallel} -dependent ARPES in this study, a single graphene layer is sufficient. The atomic potentials are generated for an infinite graphene layer using density functional theory with the LMTO code [23] in the atomic sphere approximation. The band structure (Fig. 2) is in good agreement with the literature [24]. In the atomic sphere approximation, several layers of empty spheres must be introduced in order to fill the space between repeated graphene slabs. In the MST cluster calculation, three layers of empty spheres are kept, see Fig. 1b. These empty spheres are important for describing the spatial extension of C - s and p orbitals beyond the radius of the C atomic spheres. In the atomic (C) spheres the wave function is expanded in spherical waves up to angular momentum $l = 1$ for the initial state and $l = 2$ for the final state. In the empty spheres, the maximum l -values are $l = 0$ and $l = 1$ for the initial and final state, respectively. Following the muffin-tin approximation, the potential in the interstitial space is a constant V_{MTZ} . We take $V_{\text{MTZ}} = E_B + E_F - 4.6$ eV, where E_F is the Fermi energy and $E_B < 0$ is the (negative) binding energy. For the Fermi-level ($E_B = 0$) this formula gives the same V_{MTZ} -value as that obtained in the LMTO band calculation. For $E_B < 0$, the V_{MTZ} value is lowered progressively in order to ensure that the kinetic energy in the initial state calculation is positive, which is a technical condition in the present MST implementation [22]. We also tried several fixed values for V_{MTZ} but found that the above binding energy dependent value gives best results. The optical transition matrix

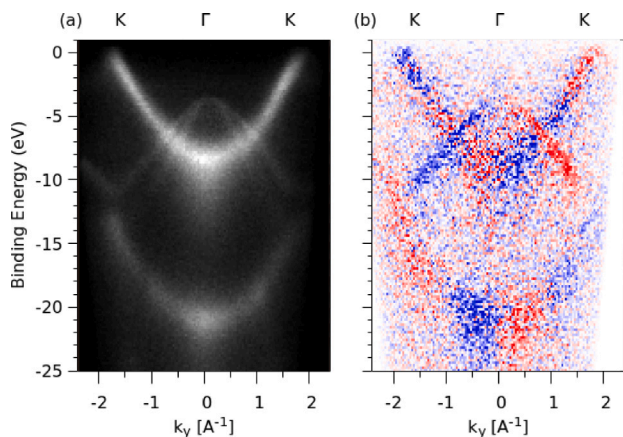


Fig. 3. Experimental ARPES of graphite for $\mathbf{k}_{\parallel} = (0, k_y)$, i.e. along the K- Γ -K line. (a) Sum of ARPES intensities for right (I_R) and left (I_L) circular polarized light. (b) CD, i.e. $I_R - I_L$. Positive, zero and negative CD shown in blue, white and red color, respectively. The maximum CD in (b) is $\pm 5\%$ of the maximum ARPES intensity in (a).

elements are computed in electric dipole approximation in acceleration form, following Pendry [13]. The weak spin-orbit coupling of carbon is neglected and the calculations are carried out disregarding electron spin. Apart from the inclusion of empty spheres, the present theoretical method is the same as the one used successfully for ARPES from metal surfaces [22,25]. In the ARPES plots below, the polar emission angle θ_e is converted to the surface parallel component of photoelectron momentum using [1]

$$\hbar k_{\parallel} = \sqrt{2m(hv - \phi + E_B)} \sin(\theta_e),$$

where $\phi = 4.6$ eV is the work function of graphite [18]. We also carry out calculations in the independent atomic center approximation (IACA) which is identical to the full MST calculations, except that final state photoelectron scattering is switched off. In practice, this is achieved simply by replacing the scattering path operator τ_{ij} by the atomic T -matrices $t_i \delta_{ij}$ in the final state calculation, see Refs. [22,26] for details. Note that the present IACA method differs somewhat from the original IACA [11], because in the latter, matrix elements were computed with free atom final state waves and the length form of the dipole operator was used.

3. Results and discussion

Fig. 3 shows the experimental ARPES map $I(k, E_B)$ for \mathbf{k}_{\parallel} vectors $(0, k_y)$, i.e. along the K- Γ -K line of the Brillouin zone. In Fig. 3a, the total ARPES intensity, i.e. the sum of intensities for right (I_R) and left (I_L) circular polarized light is shown. The visible band dispersion agrees well with the literature [18] and the DFT band structure of graphene along Γ -K (Fig. 2). Fig. 1b shows the corresponding CD map, i.e. the intensity difference $I_R - I_L$. The maximum CD is about 5% of the maximum ARPES and it has a complex band- and k -dependence. The CD signal is antisymmetric with respect to k_y , i.e. it changes sign when going from positive to negative k_y . This is easily understood from the symmetry of the problem. Photoemission at k_y with right circular polarized light is equivalent to emission at $-k_y$ with left circular polarized light. This can be seen by applying two symmetry operations of the graphite surface, namely a rotation by π about the surface normal and reflection at the yz (emission) plane. The combined operation changes the emission direction from (k_x, k_y, k_z) to $(k_x, -k_y, k_z)$ and switches right to left circular polarization while keeping the incident light direction unchanged. Apart from this symmetry property, the CD signal shows several other, non-trivial sign changes, either as a function of band index for fixed k , or, in the case of bands No 1 and 4, in the same band at a particular k -value between Γ and K.

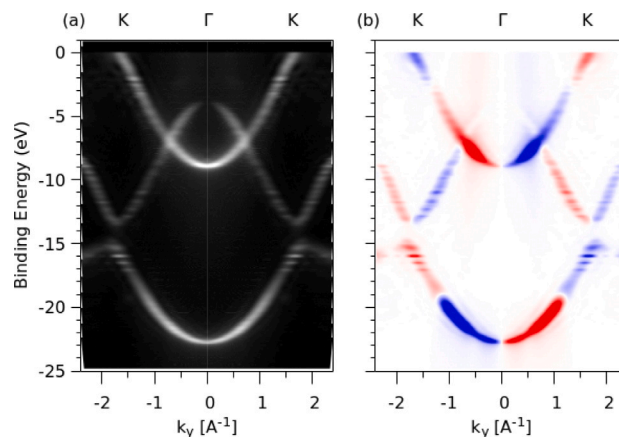


Fig. 4. Theoretical ARPES (a) and its CD (b) along $(0, k_y)$, i.e. the K- Γ -K line obtained with MST. The maximum CD in (b) is $\pm 20\%$ of the maximum ARPES intensity in (a).

The calculated ARPES for $\mathbf{k}_{\parallel} = (0, k_y)$ is shown in Fig. 4a. The dispersion of the occupied bands No. 1,3,4 are well reproduced. Only band No. 2 is not visible. Note that also in the experimental ARPES map, band No. 2 is very weak and hardly visible for $|k_y| > 1 \text{ \AA}^{-1}$. The intensity variations of the calculated bands agree well with the data in Fig. 3a. This shows that the real-space MST method provides an accurate description of the ARPES spectra, not only for closed packed metals [22], but also for covalent bonded systems and 2D materials.

The calculated CD is shown in Fig. 4b. It is more intense and more concentrated on the bands than the experimental CD (Fig. 3b). This may be due to limited instrumental resolution, the incomplete polarization (70%) in the experiment and inelastic scattering effects. Apart from this quite common difference between measured and calculated data, the theoretical CD map agrees very well with the experimental one. In particular, the sign changes of the CD between different bands, and within the same band as a function of k , are very well reproduced. In Fig. 5, the experimental ARPES and CD are shown after rotating the sample clockwise by 90° about the surface normal. In the sample frame, light is now incoming in the yz plane with $y < 0$ and photoelectrons are emitted in the xz plane. Momenta $\mathbf{k}_{\parallel} = (k_x, 0)$, i.e. along the M- Γ -M line are probed. The corresponding calculations are shown in Fig. 6. All four occupied graphene bands along Γ -M are clearly seen in both the experimental and the theoretical ARPES maps. Also the mirror symmetry of the band dispersion at the M point is evident, especially in the theoretical ARPES. As for the Γ -K line, the agreement between theory and experiment is very good, both for the ARPES and the CD intensity map. When comparing the CD maps along Γ -K (Fig. 3b) and Γ -M (Fig. 5b), the overall intensity distribution is similar, which seems to reflect the fact that the band structure and the total ARPES intensity maps are fairly isotropic, see Figs. 2, 3a, 5a. The bands No 3 (Γ -K) and No 2' (Γ -M) have similar dispersion and ARPES intensities, but while the CD of band No 3 is large, that of band No 2' is very weak. These differences can also clearly be observed in the calculated CD maps (Figs. 4b, 6b).

In order to better understand the origin of the strong CD, we computed the ARPES also in the IACA, i.e. by switching off all final state scattering. ARPES and CD along Γ -K are shown in Fig. 7. The overall intensity is somewhat smaller than in MST. (Note that an enhanced color scale is used in Fig. 7.) The band dispersion is unchanged, since the initial state calculation is the same in the two methods. The final states are different and so the ARPES intensities are different, but the relative intensity variations seen in the ARPES maps of Figs. 4a and 7a are very similar, and the level of agreement with experiment (Fig. 3a) is comparable for MST and IACA calculations. However, the CD map computed in the IACA (Fig. 7b) is very different from the MST result (Fig. 5b). The sign of the CD is opposite to MST and experiment for

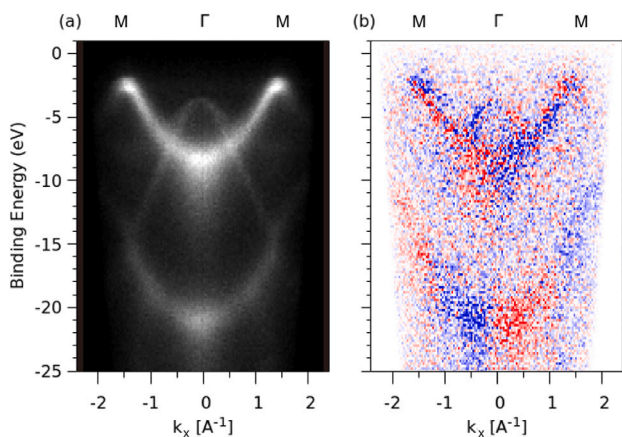


Fig. 5. Experimental ARPES (a) and its CD (b) of graphite along $(k_x, 0)$, i.e. the M- Γ -M line. The same gray/color scale as in Fig. 3 is used.

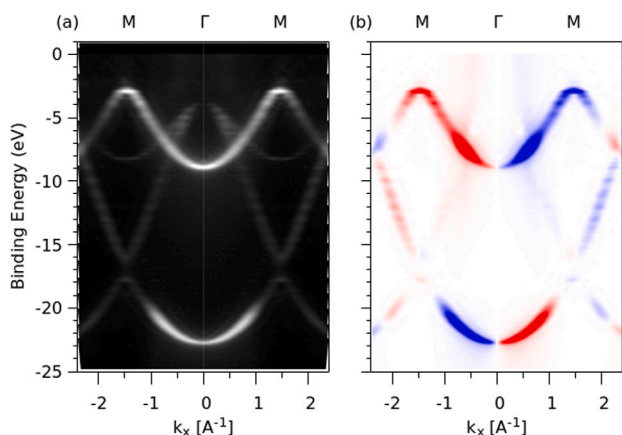


Fig. 6. Theoretical ARPES (a) and its CD (b) along $(k_x, 0)$, i.e. the M- Γ -M line obtained with MST. The same gray/color scale as in Fig. 4 is used.

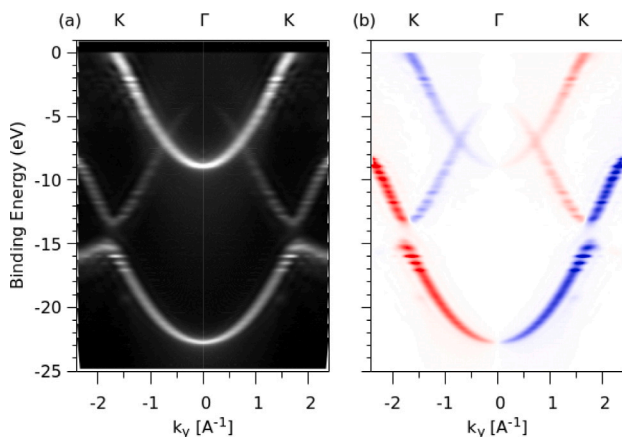


Fig. 7. Theoretical ARPES (a) and its CD (b) along $(0, k_y)$ in the IACA approximation. The gray and color scales are enhanced by a factor of 2 as compared to Figs. 4, 6.

several bands. Especially the strong CD of bands No. 1,4 around Γ (i.e. for $|k_y| < 1 \text{ \AA}^{-1}$) is not reproduced in the IACA; neither in sign nor in relative intensity. The IACA calculation for Γ -M (not shown) has the same flaws.

The foregoing comparison between the MST and IACA results shows that final state scattering effects make a large contribution to the CD and must be taken into account to reproduce the experimental data.

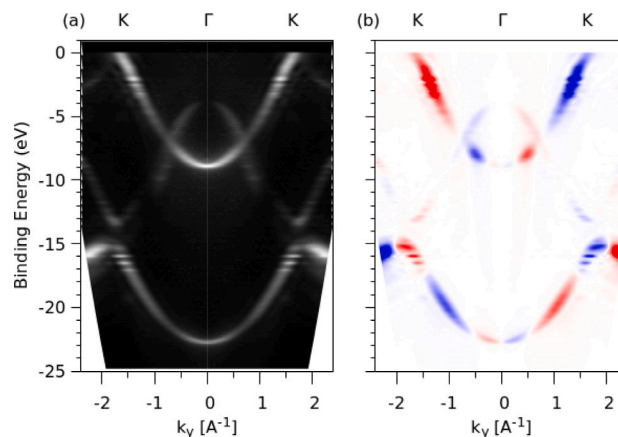


Fig. 8. Theoretical ARPES (a) and its CD (b) along $(0, k_y)$ obtained with MST for a photon energy $h\nu = 50 \text{ eV}$. The gray and color scale are enhanced by a factor of 1.5 as compared to Figs. 4, 6.

The fact that photoelectron scattering can give rise to CD is well known. CD occurs for example around forward scattering peaks in X-ray photoelectron diffraction [27], known as the Daimon effect [28]. It also contributes to the CD of adsorbed molecules [29]. The absolute ARPES intensity is much less affected by photoelectron scattering as it is seen by the rather good agreement of IACA and experiment for the sum of left and right circular polarized light. One may conclude that the CD is much more sensitive to the quality of the final state wave function than the absolute ARPES intensity. This is in line with the fact that the PWA can give reasonable ARPES maps [6,10], but it fails to produce any CD [26,30].

In order to understand the effect of the photon energy, theoretical ARPES and CD maps along $(0, k_y)$ for $h\nu = 50 \text{ eV}$ are shown in Fig. 8. The ARPES map (Fig. 8a) is very similar to that for $h\nu = 80 \text{ eV}$ (Fig. 5a); some intensity changes are visible, but they do not change the overall picture. The CD map (Fig. 8b) however, is completely different from that for $h\nu = 80 \text{ eV}$ (Fig. 5b). Indeed, the CD is reversed for many bands and the maximum CD contrast is shifted from the $|k_y| < 1 \text{ \AA}^{-1}$ region to $1 < |k_y| < 2 \text{ \AA}^{-1}$. We conclude that the photon energy has a much larger effect on the CD than on the absolute ARPES intensity.

The results above show that ARPES from graphite has a complex CD which strongly depends on both the initial and final state wave functions. In order to get an idea, about what length scale of the wave functions is important for the formation of the CD contrast, we performed a model calculation with a single C6-ring, which can be considered the minimum motif of the graphene structure. The ARPES and CD maps along $(0, k_y)$, i.e. in the geometry of Fig. 1, are shown in Fig. 9. For the C6 ring, a discrete energy spectrum of the molecular orbitals is obtained instead of the continuous bands of graphene. Nonetheless, the ARPES map of the C6 ring (Fig. 9a) resembles that of graphene (Figs. 3a, 4a) in terms of the (E, k_y) [or (E, θ_e)] intensity distribution. This suggests that the molecular orbital wave functions are, on the length scale of the C6 ring, similar to the Bloch wave functions of graphene of the same energy. Comparing the CD map of the C6 ring (Fig. 9b) with that of graphene (Fig. 4b) it can be seen that the overall intensity distribution in the (E, k_y) plane is similar. In particular, the strongest CD is seen in the central region $|k_y| < 1 \text{ \AA}^{-1}$ at similar energies as the bands 1 and 4 in graphene (s -like σ -band and p_z -like π -band, respectively). This similarity suggests that the CD-contrast in ARPES is mainly generated on the length scale of the molecular bands, and that it is largely independent of band formation. Indeed, strong CD has been observed in photoemission of oriented molecules on surfaces [20,26,31]. In Fig. 9, one can notice that the k_y -positions of maximum intensity do not coincide between ARPES and CD maps. The intensity peaks of the CD map are generally shifted to the left or

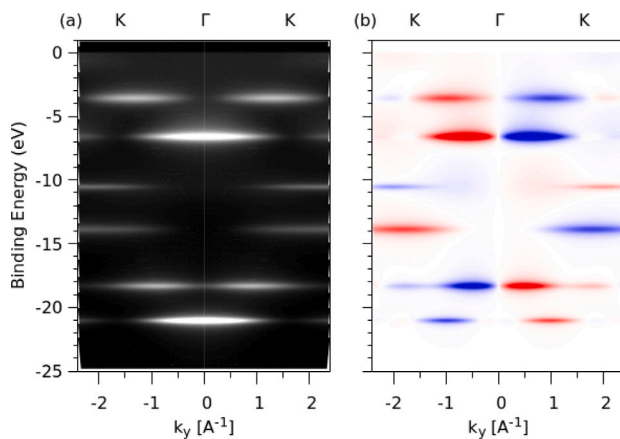


Fig. 9. Theoretical ARPES (a) and its CD (b) along $(0, k_y)$ obtained with MST for a single C6 ring.

right of the ARPES peaks, i.e. CD is strongest at the tail of an ARPES peak. This means that the ARPES peaks for left and right circular polarized light are shifted in k_y (or angle θ_e) in opposite directions. This feature is reminiscent of the forward scattering peak shift in X-ray photoelectron diffraction (Daimon effect) and it underlines once again the importance of photoelectron scattering effects for the understanding of CD in ARPES.

4. Conclusions

We have reported the observation of strong circular dichroism in ARPES from a graphite surface with photon energy 80 eV in grazing incidence. The CD map is complex; it changes sign between bands and also as a function of momentum k within the same band along the Γ -K and Γ -M lines of the Brillouin zone. Both the absolute ARPES intensity map and the CD map could be explained with theoretical calculations based on the one-step model of photoemission with a real-space MST. The band dispersion and the complex CD have been well reproduced in the calculations. By comparison with the independent atomic center approximation we have shown that photoelectron scattering effects give a large contribution to the CD, although they play a much lesser role for the absolute ARPES intensities, where the IACA may be sufficiently accurate. We also showed that the CD depends very strongly on photon energy, while much less so for the absolute ARPES intensity. The present findings clearly demonstrate that an accurate description of the photoemission final state, including photoelectron scattering, is crucial for describing the polarization dependence of ARPES spectra. This implies that an interpretation of the CD data which considers only on the initial state wave character, can easily be misleading and should be avoided.

Declaration of competing interest

The authors declare that they have no known competing financial interests or personal relationships that could have appeared to influence the work reported in this paper.

Acknowledgments

F.M. thanks Dr. Matthias Muntwiler of the Paul Scherrer Institute, Switzerland for supporting the experiment during the synchrotron radiation beam time at beamline X03DA (PEARL) of the SLS. Both authors (P.K. and F.M.) remain in grateful memory of the late Charles (Chuck) Fadley. Chuck's outstanding contributions to the field of photoelectron spectroscopy had a strong impact on our research. We met Chuck many times at conferences and had the pleasure to co-organize some workshops with him. We also had the great privilege to collaborate with Chuck at several occasions and learned a lot from this great scientist and warmhearted human being.

References

- [1] A. Damascelli, Z. Hussain, Z.-X. Shen, *Rev. Modern Phys.* 75 (2003) 473.
- [2] C. Jozwiak, C.-H. Park, K. Gotlieb, C. Hwang, D.-H. Lee, S.G. Louie, J.D. Denlinger, C.R. Rotundu, R.J. Birgeneau, Z. Hussain, A. Lanzara, *Nature Phys.* 9 (2013) 293.
- [3] C.-Z. Xu, Y. Liu, R. Yukawa, L.-X. Zhang, I. Matsuda, T. Miller, T.-C. Chiang, *Phys. Rev. Lett.* 115 (2015) 016801.
- [4] A. Winkelmann, C. Tusche, A.A. Ünal, M. Ellguth, J. Henk, J. Kirschner, *N. J. Phys.* 14 (2012) 043009.
- [5] C. Tusche, Y.-J. Chen, C.M. Schneider, J. Kirschner, *Ultramicroscopy* 206 (2019) 112815.
- [6] P. Puschnig, S. Berkebile, A.J. Fleming, G. Koller, K. Emtsev, T. Seyller, J.D. Riley, C. Ambrosch-Draxl, F.P. Netzer, M.G. Ramsey, *Science* 326 (2009) 702.
- [7] K. Sakamoto, H. Ishikawa, T. Wake, C. Ishimoto, J. Fujii, H. Bentmann, M. Ohtaka, K. Kuroda, N. Inoue, T. Hattori, T. Miyamachi, F. Komori, I. Yamamoto, Cheng Fan, P. Krüger, H. Ota, F. Matsui, F. Reinert, J. Avila, M.-C. Carmen Asensio, *Nano Lett.* 21 (2021) 4415.
- [8] R. Ono, A. Marmodoro, J. Schusser, Y. Nakata, E.F. Schwier, J. Braun, H. Ebert, J. Minár, K. Sakamoto, P. Krüger, *Phys. Rev. B* 103 (2021) 125139.
- [9] C. Metzger, M. Graus, M. Grimm, G. Zamborlini, V. Feyer, M. Schwendt, D. Lüftner, P. Puschnig, A. Schöll, F. Reinert, *Phys. Rev. B* 101 (2020) 165421.
- [10] S. Moser, *J. Electron. Spectrosc. Relat. Phenom.* 214 (2017) 29.
- [11] W.D. Grobman, *Phys. Rev. B* 17 (1978) 4573.
- [12] S. Hasegawa, S. Tanaka, Y. Yamashita, H. Inokuchi, H. Fujimoto, K. Kamiya, K. Seki, N. Ueno, *Phys. Rev. B* 48 (1993) 2596.
- [13] J. Pendry, *Surf. Sci.* 57 (1976) 679.
- [14] J. Xu, P. Krüger, C.R. Natoli, K. Hayakawa, Z. Wu, K. Hatada, *Phys. Rev. B* 92 (2015) 125408.
- [15] J. Braun, *Rep. Progr. Phys.* 59 (1996) 1267.
- [16] A. Gonis, W.H. Butler, *Multiple Scattering in Solids*, Springer-Verlag, New York, 2000.
- [17] K. Hatada, K. Hayakawa, M. Benfatto, C.R. Natoli, *Phys. Rev. B* 76 (2007) 060102(R).
- [18] T. Takahashi, H. Tokailin, T. Sagawa, *Phys. Rev. B* 32 (1985) 8317.
- [19] F. Matsui, H. Nishikawa, H. Daimon, M. Muntwiler, M. Takizawa, H. Namba, T. Greber, *Phys. Rev. B* 97 (2018) 045430.
- [20] C. Westphal, J. Bansmann, M. Getzlaff, G. Schönense, *Phys. Rev. Lett.* 63 (1989) 151.
- [21] M. Muntwiler, J. Zhang, R. Stania, F. Matsui, P. Oberta, U. Flechsig, L. Patthey, C. Quitmann, T. Glatzel, R. Widmer, E. Meyer, T.A. Jung, P. Aebi, R. Fasel, T. Greber, *J. Synchrotron. Radiat.* 24 (2017) 354.
- [22] P. Krüger, F. Da Pieve, J. Osterwalder, *Phys. Rev. B* 83 (2011) 115437.
- [23] O.K. Andersen, *Phys. Rev. B* 12 (1975) 3060.
- [24] D.W. Boukhvalov, M.I. Katsnelson, A.I. Lichtenstein, *Phys. Rev. B* 77 (2008) 035427.
- [25] F. Da Pieve, P. Krüger, *Phys. Rev. Lett.* (2013).
- [26] P. Krüger, *J. Phys. Soc. Japan* 87 (2018) 061007.
- [27] C.S. Fadley, *J. Electron. Spectrosc. Relat. Phenom.* 178–179 (2010) 2.
- [28] H. Daimon, *Phys. Rev. Lett.* 86 (2001) 2034.
- [29] G.H. Fecher, A. Oelsner, Ch. Ostertag, G. Schönense, *J. Electron. Spectrosc. Relat. Phenom.* 76 (1995) 97.
- [30] A.M. Bradshaw, D.P. Woodruff, *New J. Phys.* 17 (2015) 013033.
- [31] M. Dauth, M. Graus, I. Schelter, M. Wiener, A. Schöll, F. Reinert, S. Kümmel, *Phys. Rev. Lett.* 117 (2016) 183001.